JMEPEG
https://doi.org/10.1007/s11665-026-14047-y

1059-9495/$19.00

ORIGINAL RESEARCH ARTICLE

Frictional Frequency-Dependent Tribocorrosion Behaviors of Atmospheric Plasma-Sprayed FeCoCrNiMn High-Entropy Alloy Coatings in Simulated Seawater

Fuyang Cao, Mingming Zhang, Hang Wang, Weixuan Sun, Yingqi Sun, Haoquan Wang, Hengnan Ding, Fei Wang, Rui Luo, and Yu Liu

Submitted: 1 March 2026 / Revised: 9 April 2026 / Accepted: 16 April 2026

FeCoCrNiMn high-entropy alloy coatings were deposited on 304 stainless steel substrates via atmospheric plasma spraying, and the tribocorrosion wear behaviors of these FeCoCrNiMn high-entropy alloy (HEA) coatings in 3.5 wt.% NaCl solution at various frictional frequencies were investigated. The as-sprayed coating exhibited a typical FCC structure. The hardness of the HEA coating was 221.1 HV0.2, which was 39.0% higher than the substrate. During the tribocorrosion test, both the friction coefficient and wear rate increased as the frictional frequency increased from 0.5 to 2 Hz. The self-corrosion current density increased from 1.28×10^{-7} A cm^{-2} at static state to 1.22×10^{-5} A cm^{-2} at 2 Hz, and self-corrosion potential shifted negatively from − 0.35 to − 0.45 V as the frictional frequency increased from 0.5 and 2 Hz. These behaviors were attributed to enhanced mechanical depassivation and insufficient re-passivation with increasing frequency. The main wear mechanism was dominated by fatigue wear, together with an enhanced abrasion at higher frequencies. Quantitative analysis of the corrosion–wear synergy showed that the proportion of the wear-accelerated corrosion increased from 1.6 to 6.5% due to an increased frictional frequency.

Keywords frictional frequency, high-entropy alloy coating, tribocorrosion, synergistic effect

1. Introduction

The service safety and longevity of marine engineering equipment are critically threatened by the synergistic degradation of corrosion and mechanical wear (Ref 1-7). Conventional protective coatings, including stainless steel and nickel-based alloys, are often inadequate due to their limited ability to concurrently provide high hardness and exceptional corrosion resistance (Ref 8). Consequently, developing new coatings that simultaneously offer superior corrosion and wear resistance has become a critical priority in marine engineering.

Fuyang Cao, School of Materials Science and Engineering, Jiangsu University, Zhenjiang 212013, China; and State Key Laboratory of High Performance Tools, Chengdu 610599, China; **Mingming Zhang, Weixuan Sun, Yingqi Sun, Haoquan Wang, Fei Wang,** and **Rui Luo**, School of Materials Science and Engineering, Jiangsu University, Zhenjiang 212013, China; **Hang Wang**, School of Materials Science and Engineering, Jiangsu University, Zhenjiang 212013, China; and Jiangsu Jitui Advanced Metal Materials Research Institute Co., Ltd., Changshu 215558, China; **Hengnan Ding**, School of Agricultural Engineering, Jiangsu University, Zhenjiang 212013, China; and **Yu Liu**, School of Materials Science and Engineering, Jiangsu University, Zhenjiang 212013, China; and Jiangsu Key Laboratory of Advanced Structural Materials and Application Technology, Nanjing Institute of Technology, Nanjing, China. Contact e-mail: fuyangcao@ujs.edu.cn.

High-entropy alloys (HEAs), as a novel multi-principal element alloy system, consist of five or more elements in approximately equiatomic ratio. They have been demonstrated to possess many promising properties such as high hardness (Ref 9, 10), excellent high temperature strength (Ref 11), great wear and oxidation resistance (Ref 12-14) and excellent corrosion resistance (Ref 15, 16), which make them ideal candidate materials for marine protection. Compared with the cost and difficulty of producing large and defect-free HEA components, applying HEA coatings to the designated components offers a more feasible and cost-efficient solution with desired overall properties (Ref 17). In addition, their composition can be easily adjusted according to specific marine environment requirements. For example, the CuCoCrFeNi high-entropy alloy coating with Ag addition can not only resist seawater corrosion but also inhibit microbial adhesion and reduce biocorrosion risks (Ref 18).

In recent years, the performance of high-entropy alloy coatings in marine environments has been widely studied. For instance, Argade et al studied the tribocorrosion performance of AlCoCrFe HEA coating in 0.6 M NaCl solution and found that the wear volume loss of the coating was 10 times lower than that of the aluminum substrate (Ref 19). Similarly, the detonation-sprayed $CrFeNiAl_{0.3}Ti_{0.3}$ HEA coating exhibited higher corrosion resistance than the SUS304 substrate in a seawater environment (Ref 20). Liang et al. (Ref 21) studied the tribological properties of $AlCrFeNiW_{0.2}Ti_{0.5}$ high-entropy alloy coating in seawater and found that the coating showed a low friction coefficient (0.15) and wear rate (4.5×10^{-7} mm^3/Nm) when paired with YG6 steel due to the protective film (composed of metal oxides and hydroxides) formed on the coating surface during friction. Lu Li et al. studied the corrosion–wear behavior of HVOF-deposited AlCoCrFeNi

Published online: 03 May 2026

coating in seawater and found that under the corrosion–wear coupling effect, corrosion and wear promoted each other, and the effect of corrosion-accelerated wear was greater than the effect of wear-accelerated corrosion (Ref 22). Our group previously compared the tribocorrosion wear behaviors of atmospheric plasma-sprayed FeCoCrNiMn HEA coatings in both 3.5 wt.% NaCl solution and deionized water under different loads. We found that the difference of wear volume loss in deionized water under different loads was smaller than that of wear volume loss in 3.5 wt.% NaCl solution, indicating that the corrosive wear media played a significant role in the synergistic effect between corrosion and wear (Ref 23). To date, however, there are limited studies regarding the effect of frictional frequency on the tribocorrosion wear behavior of HEA coatings, and the related synergistic mechanism is still unclear.

In this work, a number of FeCoCrNiMn HEA coatings were worn in 3.5 wt. % NaCl solution at various frictional frequencies. The tribocorrosion behaviors, surface morphology and composition were characterized and compared, to explore the effect of frictional frequency on the wear mechanism and its influence on the corrosion–wear synergistic effect.

2. Experimental Procedures

Commercial Fe, Co, Cr, Ni and Mn powders (purity ≥ 99.8%) with a nominal particle size of 45-150 μm were selected as the raw material. These powders with a mole ratio of 1:1:1:1:1 were homogeneously mixed using planetary ball milling. The 304 stainless steel with a dimension of 200 × 100 × 3 mm was selected as the substrate material, which was first ground with sandpaper and then underwent sandblasting treatment. Afterward, the pre-treated substrates were ultrasonically cleaned with acetone and ethanol solutions separately and dried by hot air for subsequent use.

An atmospheric plasma spraying system (Metco FaMB90-XL) was employed to fabricate an equiatomic HEA FeCoCrNiMn coating. In order to reduce oxidation during spraying, argon (Ar) was selected as the primary gas, hydrogen (H_2) as the secondary gas and nitrogen (N_2) as the powder-feeding gas. The detailed spraying parameters are shown in Table 1.

The coatings were then sectioned into square samples of 10 × 10 mm. And the HEA coating surface of the samples for tribocorrosion tests was carefully ground with SiC sandpaper to grade 1500 and polished with a 0.25-μm polycrystalline diamond suspension to achieve a mirror surface. Subsequently, the samples were ultrasonically cleaned in ethanol and dried in air.

The tribocorrosion tests were carried out in a three-electrode cell on a reciprocating sliding tribometer (MFT-EC4000, Lanzhou Huahui Co., Ltd. China). The three-electrode configuration consists of an Ag/AgCl with saturated KCl as the reference electrode, a graphite rod as the counter electrode and the above-mentioned HEA coating samples as the working electrodes. The HEA coating samples were fixed on a Teflon cell, using a Teflon mask and fluorosilicone sealant, ensuring that only the HEA coating surface was exposed to the corrosive medium. All the tests were conducted in simulated sea water, 3.5 wt.% NaCl solution at room temperature. The applied normal load was 15 N, and the stroke length was 5 mm. Three reciprocal frequencies (0.5, 1 and 2 Hz) were applied. A Si_3N_4 ceramic ball with a diameter of 6 mm was used as the counterbody.

Before the load and potential were applied, samples were immersed in the solution for at least 30 min to obtain a stable open-circuit potential (OCP). All tests were initiated with a loading to 15 N and 300 s of stabilization at the test electrochemical condition, followed by 1200 s of sliding at each frequency and a further 300 s of monitoring the electrochemical parameter after the cessation of sliding. The dynamic friction coefficient was recorded simultaneously at the onset of sliding. Moreover, the tribocorrosion tests with the same conditions, except an applied cathodic protection potential of − 1.0 V versus Ag/AgCl, were carried out to obtain the pure mechanical wear loss. In addition, potentiodynamic polarization scans were executed from − 0.5 to 1.5 V with respect to the OCP value at 300 s, at a scan rate of 1 mV/s. Dynamic polarization data were recorded at the onset of friction. For comparative purposes, static polarization data were recorded on the sample just after the 300-s stabilization stage. All the tests were repeated three times to ensure repeatability.

The surface roughness of the HEA coating before and after polishing was measured using a laser confocal microscope (LEXT OLS4100, Olympus). The crystal structure of the HEA coating was investigated using a Rigaku D/max-2500/pc x-ray diffractometer with Cu Kα radiation (λ = 1.54060 Å), operating at 40 kV and 200 mA. The 2θ scan range was 30°-110° at a scanning speed of 5°/min. The hardness of both the HEA coating and substrate was determined on the cross-sectional plane of the sample within an interval of 20 μm, using a Falcon 500 Vickers hardness tester (INNOVA TEST) with a load of 200 g and a dwell time of 10 s.

The cross-sectional microstructure and the wear track morphology of the HEA coating were observed by a Phenom XL G2 scanning electron microscope (SEM), and the elemental composition analysis was performed using an energy-dispersive spectrometer (EDS) attached to SEM. The cross-sectional profiles of the wear tracks were measured using the profilometry module of the MFT-4000 multifunctional material surface performance tester (Lanzhou Huahui Instrument Technology Co., Ltd.), and the corresponding cross-sectional areas were obtained from these profiles. The wear volume was calculated by the formula $V = SL$, where V is the wear volume of the material (mm^3), S is the cross-sectional area of the wear track (mm^2), and L is the wear track length (mm); the wear rate was calculated by the formula (Ref 24) $W = \frac{V}{Fd}$, where W is the

Table 1 Processing parameters for the FeCoCrNiMn HEA coating deposition

Ar flow rate, L/min	H_2 flow rate, L/min	N_2 flow rate, L/min	Powder feed rate, g/min	Spraying power, kW	Gun transverse speed, mm/s	Standoff distance, mm
50	6	8	30	30	100	120

wear rate ($mm^3\ N^{-1}\ m^{-1}$); V is the wear volume (mm^3); F is the load (N); d is the total sliding distance (m).

3. Results

Figure 1(a) shows the XRD pattern of the as-prepared FeCoCrNiMn HEA coating. It is clear that the as-prepared coating possesses a simple FCC crystal structure. Fig. 1(b) presents the cross-sectional morphology of the as-sprayed HEA coating. According to Fig. 1(b), the as-sprayed HEA coating is $\sim 160\ \mu m$ in thickness with a relatively rough surface. And a blurry interface between the coating and substrate can be identified, indicating good interfacial adhesion. Besides the pores within the coating, there exhibits a typical lamellar structure, which is characteristic of thermal sprayed coatings. During the spraying process, the semi-molten particles lead to insufficient flattening after impacting the substrate, thus randomly accumulating to form irregular shaped poles. Table 2 gives the hardness values of both the substrate and coating. It can be easily calculated that the hardness of the as-sprayed HEA coating is 39.0% higher than that of the substrate.

Figure 2 presents the surface morphology and corresponding surface roughness (Sa) of the HEA coatings before and after polished. As expected, the as-sprayed HEA coating has a relatively rough surface with a Sa value of 11.81 μm, as shown in Fig. 2(a). After careful polishing, a flat surface with a Sa value of 1.76 μm (Fig. 2b) was obtained. The subsequent tribocorrosion tests were actually performed on these polished and cleaned samples.

Figure 3 shows the potentiodynamic polarization curves of FeCoCrNiMn HEA coating under static and dynamic tribocorrosion conditions in 3.5 wt.% NaCl solution. Under static corrosion condition, the sample quickly enters into the passivation region (Region I) as the potential shifts positively. And the anodic current density no longer increases significantly with increasing potential, maintaining at about 3.44×10^{-5} A cm^{-2}. When the potential continuously increases to 0.5 V, the anodic polarization current density increases rapidly (denoted as Region II), indicating that the passive film begins to degrade. However, when the anodic polarization potential increases to 0.95 V, the anodic polarization current density of the sample maintains at about 2.80×10^{-2} A cm^{-2}, showing a re-passivation state (Region III). In contrast, under dynamic tribocorrosion conditions, higher anodic polarization current density and lower potential inflection points appear in all stages of polarization, indicating deteriorated corrosion performance and higher corrosion rate. For the tribocorrosion test done at 0.5 Hz, the anode branch curve can be divided into pseudopassivation, transpassivation and re-passivation regions. Within the pseudopassivation region, the anodic polarization current density ranges from 6.16×10^{-4} to 1.10×10^{-3} A cm^{-2}. And the anodic polarization current density stabilized at 2.17×10^{-2} A cm^{-2} in the re-passivation region. Moreover, the current densities in the passivation region for the tribocorrosion tests at 1 and 2 Hz are 1.36×10^{-3} and 1.76×10^{-3} A cm^{-2}, respectively. In the final re-passivation stage, the current density is 7.66×10^{-2} A cm^{-2} for the tribocorrosion test undertaken at 1 Hz frictional frequency and 1.10×10^{-1} A cm^{-2} for 2 Hz tribocorrosion test. Table 3 presents the self-corrosion current density i_{corr} (A/cm^2) obtained using Tafel extrapolation method for the HEA coating under static and dynamic corrosion–wear conditions. In accordance with Table 3, the corrosion current

Table 2 Microhardness of both the HEA coating and substrate

Hardness	HV0.2
As-sprayed coating	221.1
304 stainless steel	159.1

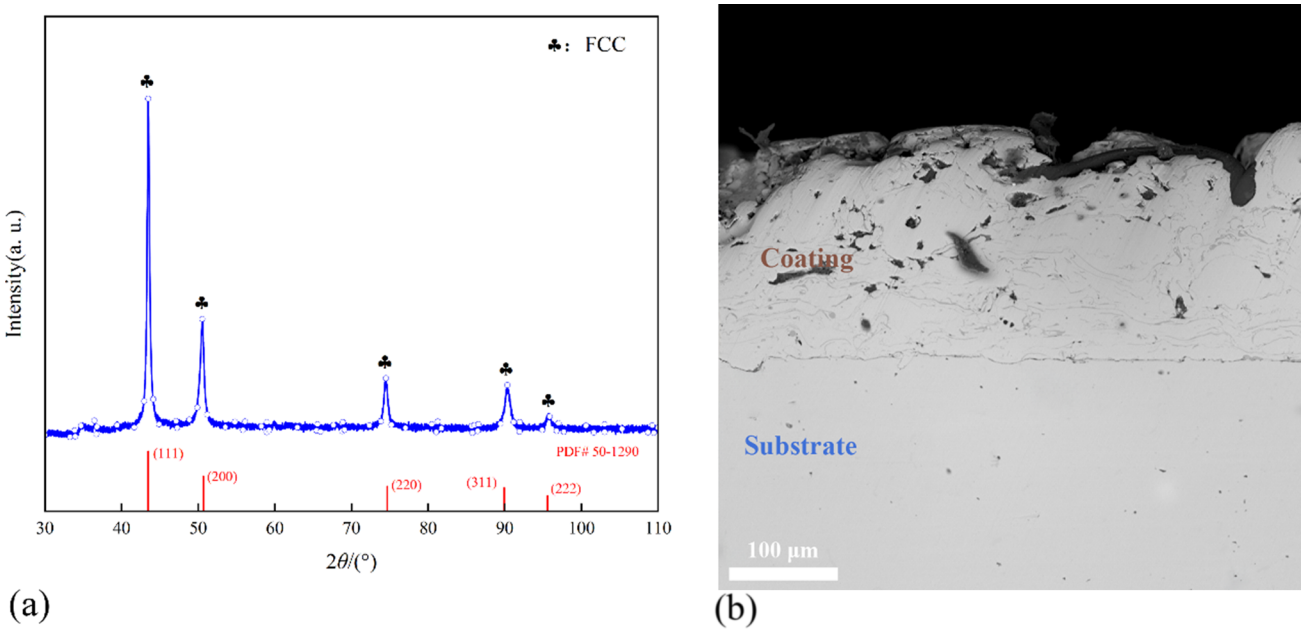

Fig. 1 XRD pattern (a) and cross-sectional SEM image of the as-prepared FeCoCrNiMn HEA coating

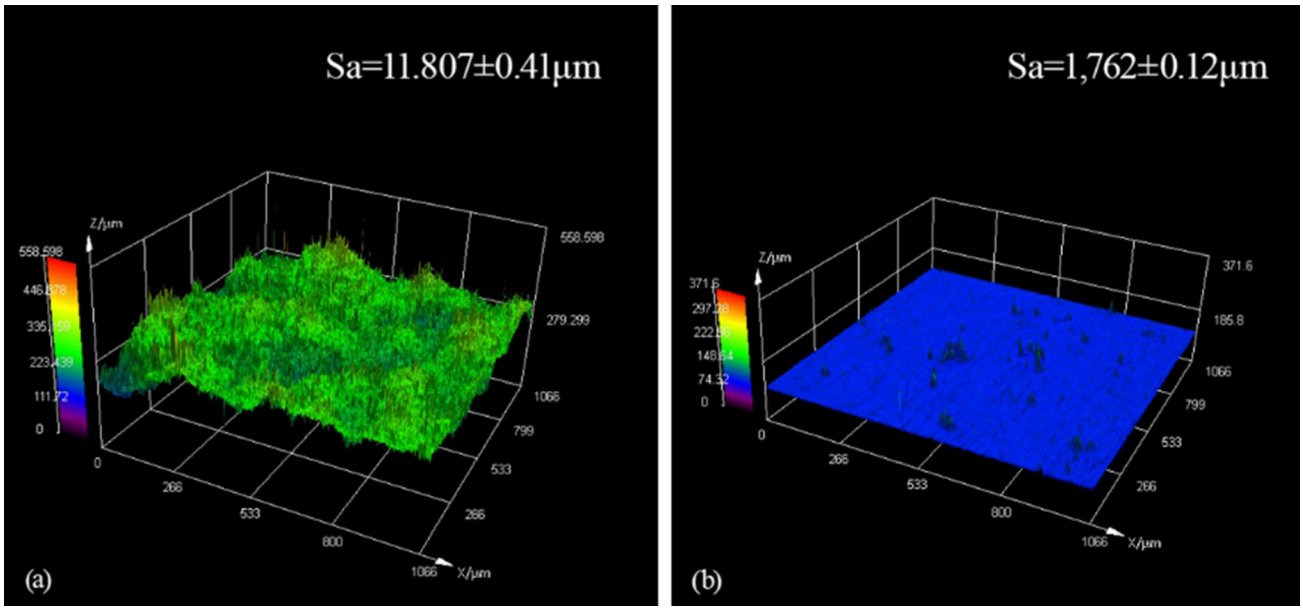

Fig. 2 Three-dimensional surface morphology of the as-sprayed (a) and polished (b) HEA coating

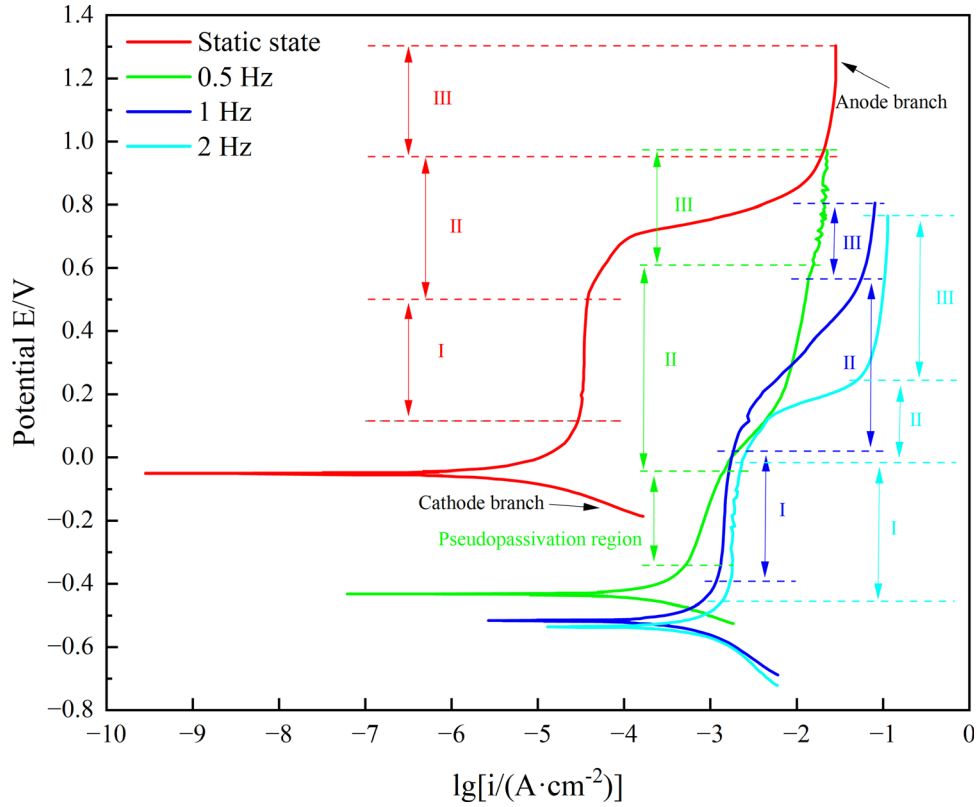

Fig. 3 Potentiodynamic polarization curve of the HEA coatings under static state and dynamic conditions with different frictional frequencies

Table 3 Self-corrosion current density of the HEA coatings in 3.5 wt.% NaCl solution obtained by Tafel extrapolation method

Condition	Static state	0.5 Hz	1 Hz	2 Hz
i_{corr}/A cm^{-2}	1.282×10^{-7}	2.138×10^{-6}	6.353×10^{-6}	1.221×10^{-5}

density i_{corr} increases with increasing frictional frequency, indicating accelerated corrosion rate.

Figure 4 shows the open-circuit potential (OCP) of the FeCoCrNiMn HEA coatings before, during and after the sliding process. Clearly, the OCP curves can be divided into three regions: the immersion region before sliding (Region I, duration 0-300 s), the sliding region (Region II, duration 300-1500 s) and the recovering region after sliding (Region III, duration 1500-1800 s). In Region I, the OCP values for all samples were maintained at around − 0.10 V, demonstrating the passive film on the HEA coating surface is in a stable state and capable of bearing a certain load. Upon the commencement of sliding (Region II), the OCP of all samples exhibits an abrupt drop. This phenomenon can be attributed to mechanical depassivation, resulting in the exposure of the active material surface to the corrosive medium. Subsequently, the OCP values were maintained at a relatively stable level for the tribocorrosion undertaken at 0.5 and 2 Hz, which were recorded as − 0.34 and − 0.46 V, respectively. While for the 1 Hz tribocorrosion test, the OCP value gradually declined to − 0.43 V after the initial sharp drop. In general, a negative shift trend of the OCP value in Region II was observed. This might suggest an increased degree of depassivation and an enhanced corrosion propensity within the wear track as a result of increasing frictional frequency. After the cessation of the sliding (Region III), the OCP rapidly recovers and finally stabilizes at − 0.16, − 0.20 and − 0.25 V for the tribocorrosion conducted at the frictional frequency of 0.5, 1 and 2 Hz, respectively. These OCP values are slightly lower than the initial OCP value before the commencement of sliding of − 0.1V, indicating enhanced localized corrosion at the HEA coating surface.

Figure 5 shows the friction coefficient curves of the FeCoCrNiMn HEA coatings versus time at different frictional frequency in 3.5 wt.% NaCl solution. According to Fig. 5, an instant drop in friction coefficient value at the onset of sliding can be seen for the tribocorrosion tests at all frequencies. This might be attributed to the transition from static to kinetic friction, and the static friction force is usually larger than the kinetic friction force (Ref 25). Subsequently, a relatively low friction coefficient between 0.03 and 0.06 among different frictional frequencies, was maintained for a period of time. During this period of time, it is believed that the sliding was actually working on the passive layer (of several nanometers (Ref 26)) under the lubricant effect of 3.5 wt.% NaCl aqueous solution. And a high frictional frequency means a quick worn-out of this protective layer. Afterward, the friction coefficient of all samples increases rapidly during the running-in stage, due to increasing contact area. For the 0.5 Hz tribocorrosion test, the friction coefficient value quickly increased to ∼ 0.21 after the running-in stage, followed by a successive drop-and-recover phenomenon, and finally stabilized at around 0.24. A similar scenario was found for the tribocorrosion test undertaken at 1 Hz, while for the 2 Hz tribocorrosion test, the friction coefficient gradually increased to ∼ 0.30 after the running-in stage, though, with a certain extent of fluctuation.

Figure 6(a) shows the cross-sectional profiles of the wear tracks in 3.5 wt. % NaCl solution at different frequencies. It can be observed that both the width and depth of the wear track increase with increasing frictional frequency. As the frequency increases from 0.5 to 2 Hz, the profile width increases from 352.0 to 403.8 μm, while the depth increases from 3.64 to 4.82 μm. Correspondingly, the calculated wear volume increases from 4.08×10^{-3} to 6.22×10^{-3} mm^3, and the calculated wear rate increases from 5.43×10^{-2} to 8.32×10^{-2} $mm^3\ N^{-1}\ m^{-1}$ in accordance with Fig. 6(b).

Figure 7 shows the surface morphologies of the wear tracks after tribocorrosion testing in 3.5 wt.% NaCl solution at different frequencies. The wear track for the HEA coating subjected to tribocorrosion at 0.5 Hz was almost covered by the flake-type debris. Besides, there was clear evidence of delamination and corrosion pits, as indicated in Fig. 7(a). As the frictional frequency increased, microgrooves could be observed in both Fig. 7(b) and (c), except for the above-mentioned flake-type wear debris, delamination and corrosion pits. The coverage of the wear track of the 1 Hz tribocorrosion by the flake-type wear debris was declined. Notably, at the highest frictional frequency of 2 Hz, the density of flake-type debris was reduced markedly, accompanied by the appearance of granular wear debris, as shown in Fig. 7(c). In addition, material spalling became more severe, which might indicate the occurrence of fatigue wear.

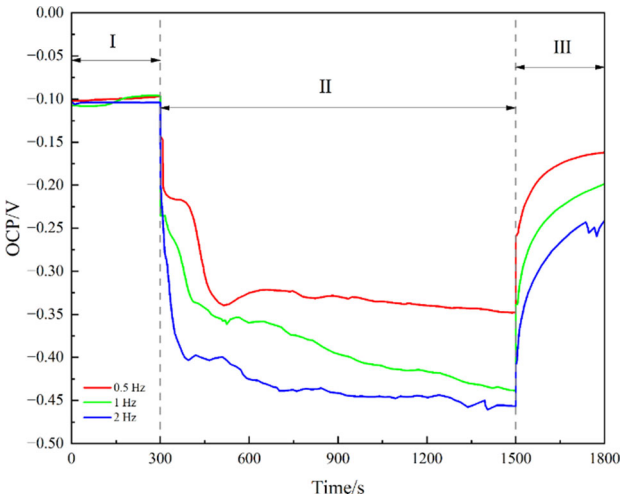

Fig. 4 Open-circuit potential of the HEA coatings during the tribocorrosion test at different frequencies in 3.5wt. % NaCl solution

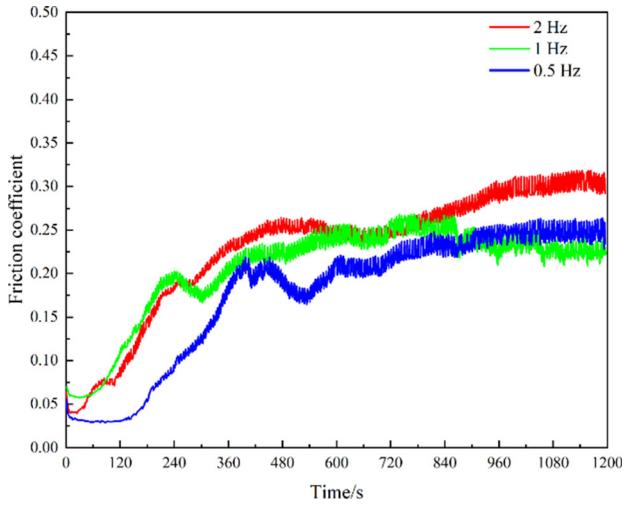

Fig. 5 Friction coefficient curves of the HEA coatings in 3.5% NaCl solution at different frequencies

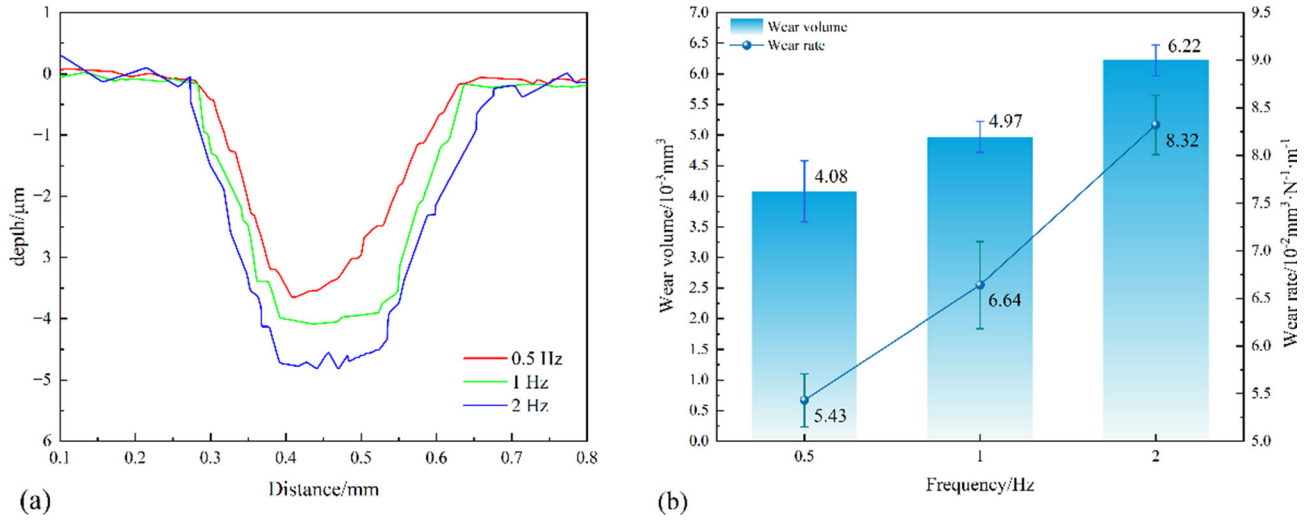

Fig. 6 Cross-sectional profiles of the wear tracks (a), wear volume and wear rate distribution (b) of the sprayed HEA coatings in 3.5% NaCl solution at different frequencies

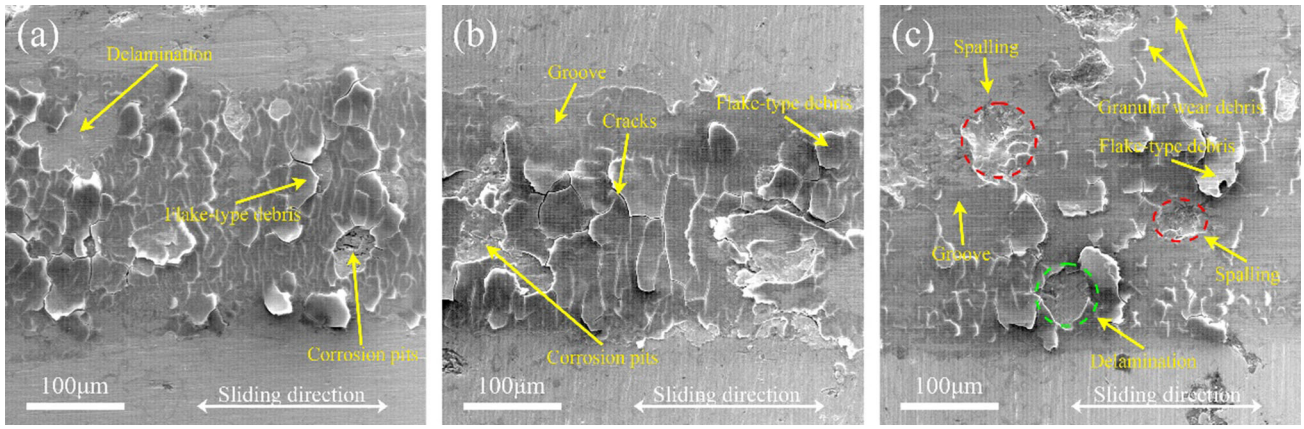

Fig. 7 The surface morphology of the wear tracks for the tribocorrosion tests conducted at different frictional frequencies in a 3.5 wt.% NaCl solution: (a) 0.5 Hz, (b) 1 Hz and (c) 2 Hz.

The elemental composition of the wear tracks tested at different frequencies was investigated by SEM-EDS. Considering the similarity in their surface morphologies, for brevity, the elemental mapping for the wear track of the 2 Hz tribocorrosion test in 3.5 wt.% NaCl solution is presented, as shown in Fig. 8. According to the Cr and O maps, it is believed that the flake-type wear debris mainly consists of chromium-rich oxides. This might also be applicable to the flake-type wear debris observed in Fig. 7(a) and (b).

4. Discussion

According to Fig. 3 and Table 3, the FeCoCrNiMn HEA coating exhibits a relatively high corrosion potential and wide passivation range, along with a low self-corrosion current density (i_{corr}) of 1.28×10^{-7} A/cm^2 under static corrosion condition. This indicates that the FeCoCrNiMn HEA coating demonstrates remarkable spontaneous passivation behavior and exceptional corrosion resistance. Upon sliding, the corrosion potential shifts in the negative direction and increases from − 0.05 V under static condition to − 0. 43 V at 0.5 Hz. Meanwhile, the corrosion potential increases to − 0.54 V with increasing frictional frequency. Simultaneously, the i_{corr} increases by one to two orders of magnitude, reaching 1.22×10^{-5} A/cm^2. This is because under tribocorrosion conditions, the thin passive film is mechanically removed by the friction pair when friction occurs, leading to the exposure of the bare metal to the NaCl solution. This process is also called mechanical depassivation. And an increase in frictional frequency shortens the interval between two consecutive wear events, leaving insufficient time for the damaged passive film to self-repair via re-passivation. As a result, the fresh FeCoCrNiMn HEA with a much more negative potential is constantly exposed to the corrosive medium. Since the overall surface potential of the sample is dominated by the exposed active matrix, an increase of friction frequency leads to a negative shift of the corrosion potential in the potentiodynamic polarization curve (as shown in Fig. 3).

In addition, according to previously published literature (Ref 27), a high friction frequency intensifies the mechanical impact and plastic deformation on the contact area, which will induce the formation of dislocation tangles, grain refinement and

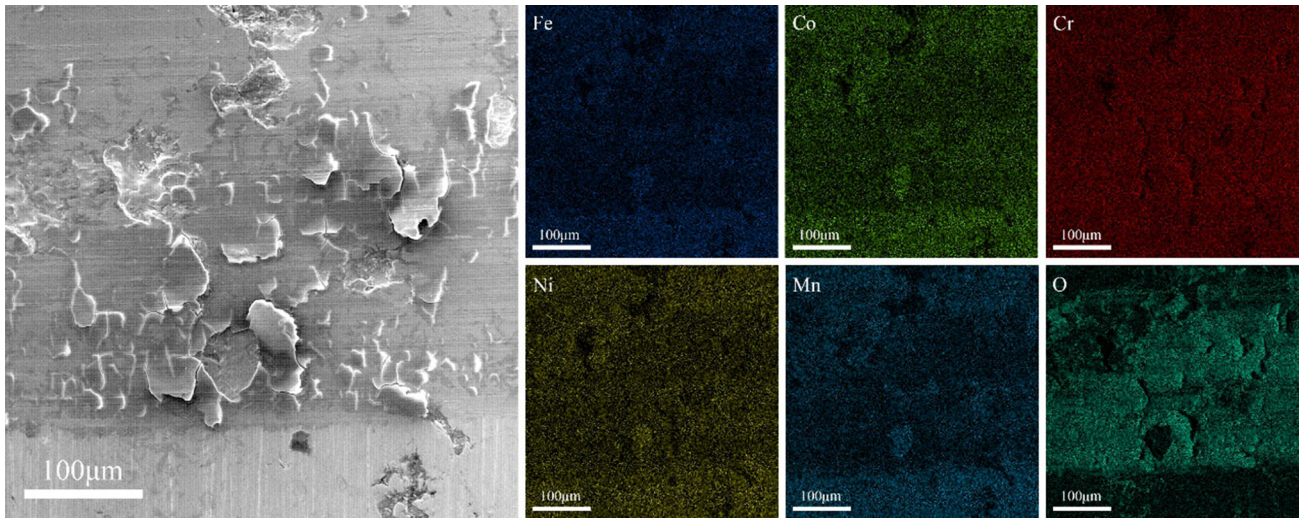

Fig. 8 SEM-EDS elemental mapping for the wear track of a 2 Hz tribocorrosion test in 3.5 wt.% NaCl solution

surface defects (e.g., microcracks) in the subsurface layer of the HEA coating. These structural defects may act as preferential sites for anodic dissolution, because of high chemical activity and low binding energy, which reduce the energy barrier for corrosion reactions and further drive the corrosion potential to shift negatively.

In fact, the aforementioned explanation for the corrosion potential drop with increasing frictional frequency, is well applicable for the decline in OCP values during the sliding stage, observed in Fig. 4. It is well established that during tribocorrosion, a galvanic couple forms between the worn area (anode) and the passive zone surrounding it. A higher frictional frequency indicates an increased degree of depassivation and enhanced corrosion kinetics and, thus, a pronounced negative shift in OCP at higher frequency. Our results are consistent with published literature, where the tribocorrosion behaviors of Ti6Al4V were studied in seawater under different frictional frequencies (Ref 28). Following the cessation of the sliding, however, the OCP does not fully recover to the initial value, which might be due to the permanent damage created on the HEA coating surface.

In terms of the COF during tribocorrosion tests, the initial sliding occurs primarily on the passive film, alongside the lubricant effect of aqueous solution. Therefore, a very low COF value was observed at the beginning of friction motion. As sliding proceeds, the cyclic stress causes the brittle passive film to crack and spall off at some points, leading to the direct contact between the HEA coating surface and the counterface. However, at low frequency, 0.5 Hz in specific, re-passivation can partially repair the ruptured passive film, resulting in a delay of the running-in period, as shown in Fig. 5, while, for the tribocorrosion tests undertaken at 1 and 2 Hz, the short interval between friction cycles is insufficient for the passive film to be generated. And thus, a shorter running-in period was observed. Following the running-in period, the subsequent decrease in COF might be due to the formation of a lubricious tribolayer, consisting of wear debris, oxide products and/or corrosion products (Ref 29). Since the wear debris generated is loose and non-adherent, a continuous, load bearing layer cannon form in the wear track. And the loose debris may act as abrasive particles, leading to the formation of microgrooves, as evidenced in Fig. 7(b) and (c). After a certain period of sliding, the surface conditions of the HEA coatings gradually stabilize, and the COF maintains at a relatively stable value. Nonetheless, the stabilized COF value of the HEA coating subjected to 2 Hz tribocorrosion test was higher than those at lower frequencies.

This behavior can be attributed to several factors. At 2 Hz, the interval between two consecutive sliding events is shorter, which leaves less time for passive-film reformation and for the development of a compact and stable tribolayer. At the same time, the higher sliding frequency intensifies repeated asperity interactions and passive-film rupture, thereby increasing the extent of direct contact between the counterbody and the coating surface. In addition, the loose wear debris generated at higher frequencies can act as third-body abrasive particles, promoting microgrooving and abrasive interaction. These combined effects result in a higher stabilized COF at 2 Hz than at lower frequencies.

However, it should be noted that there are some pores in the as-sprayed HEA coating (as shown in Fig. 1b). According to published literature (Ref 30), these pores may provide channels for solution penetration and become preferential sites for localized corrosion after the passive film is damaged during sliding. At the same time, under repeated friction, they may act as stress concentration sites, thereby promoting crack initiation and local material spalling.

The total material loss (V_T) during tribocorrosion can be calculated by the following equation (Ref 31):

$$V_T = V_W + V_C + \Delta V_W + \Delta V_C \quad \text{(Eq 1)}$$

where V_T refers to the total material loss, V_W is the pure mechanical wear, V_C is the pure corrosion. The synergistic effect of wear and corrosion is comprised of corrosion-accelerated wear (ΔV_W) and wear-accelerated corrosion (ΔV_C). The V_T and V_W of these coatings were calculated from the cross-sectional area of the wear tracks under the tribocorrosion conditions and the cathodic protection conditions in the 3.5 wt.% NaCl solution. V_C and ΔV_C were calculated according to Faraday's law, which is generally described by the following equation:

$$V_C = \frac{itM}{nF\rho} \quad \text{(Eq 2)}$$

Table 4 Material loss components after corrosion wear of high-entropy alloy coatings in 3.5% NaCl solution at different frequencies

Condition	V_T, mm^3	V_W, mm^3	V_C, mm^3	ΔV_W, mm^3	ΔV_C, mm^3
0.5 Hz	4.08×10^{-3}	3.86×10^{-3}	2.14×10^{-6}	1.51×10^{-4}	6.72×10^{-5}
1 Hz	4.97×10^{-3}	4.65×10^{-3}	2.14×10^{-6}	1.10×10^{-4}	2.08×10^{-4}
2 Hz	6.22×10^{-3}	5.78×10^{-3}	2.14×10^{-6}	3.40×10^{-5}	4.04×10^{-4}

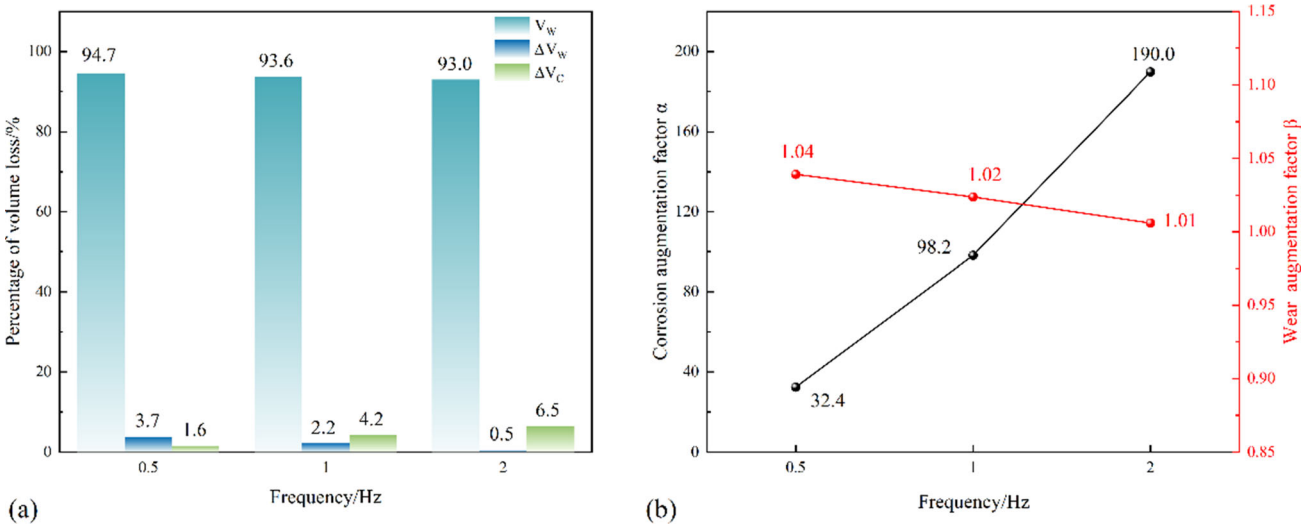

Fig. 9 (a) The contribution percentage of material loss components and (b) the corrosion and wear augmentation factors

where i is the current density, t is the total time of the sliding period, M is the molecular weight of the HEA sample (130 g/mol), F is the Faraday's constant (95485 C/mol), and ρ is the density of the HEA coating (the calculated density of the FeCoCrNiMn HEA coating was 8.06 according to the mixing law, $\rho_{HEA} = \sum_{i}^{n} (\rho_i \cdot \omega_i)$(Ref 32)). The valence ($n$) of the oxidation of the HEA coating is set to be 6 based on the fact that the oxide formed on the HEA coating surface in passivation was mainly Cr_2O_3 (Ref 33). Lastly, ΔV_W can be calculated by formula (1) after obtaining the values of V_T, V_W, V_C and ΔV_C, where are summarized in Table 4. According to Table 4, except V_C, the values of V_T, V_W, ΔV_C and ΔV_W all increase progressively with increasing frictional frequency. The V_C contribution only accounts for 0.03-0.05 % of the total material loss, which might be attributed to the excellent corrosion resistance of FeCoCrNiMn HEA coating.

Figure 9(a) shows the percentage of each individual material loss component to the total material loss at different frictional frequencies in the 3.5 wt.% NaCl solution. The ratio of V_W/V_T slightly decreases with increasing frictional frequency from 94.7 to 93.0%, indicating that the tribocorrosion was dominated by pure mechanical wear. Additionally, the ratio of the corrosion-accelerated wear (ΔV_W) to the total material loss V_T declines from 3.7 to 0.5% with the frictional frequency varying between 0.5 and 2 Hz, while the contribution of wear-accelerated corrosion (ΔV_C) to the total material loss increases with increasing frictional frequency from 1.6 to 6.5%.

Furthermore, a corrosion augmentation factor (α) and a wear augmentation factor (β) were used to analyze the influence of frictional frequency on the tribocorrosion behavior of the HEA coatings in the artificial seawater. Equations are as follows:

$$\alpha = \frac{V_C + \Delta V_C}{V_C} \quad \text{(Eq 3)}$$

$$\beta = \frac{V_w + \Delta V_W}{V_W} \quad \text{(Eq 4)}$$

The α and β of the HEA FeCoCrNiMn coatings at different frictional frequencies in tribocorrosion are shown in Fig. 9(b). Clearly, the wear augmentation factor (β) remained almost constant, with a marginal decline from 1.04 to 1.01 as the frequency increased from 0.5 to 2 Hz. In contrast, the corrosion augmentation factor (α) increased by $\sim$ 5 times, from 32.4 at 0.5 Hz to 190.0 at 2 Hz. This is due to the cyclic removal of the passive film by abrasion followed by its growth (depassivation/re-passivation mechanism), and the high frequency leaves insufficient time intervals for re-passivation. As a consequence, corrosion pitting increases markedly. In addition, in the presence of chloride, metal dissolution from sites where the passive film is locally broken will be promoted, leading to enhanced wear-accelerated corrosion.

5. Conclusions

The HEA FeCoCrNiMn coatings, fabricated on 304 stainless steel substrates using atmospheric plasma spraying, possess an FCC crystal structure. The effect of frictional frequency on the tribocorrosion behavior of these coatings in a 3.5 wt.%

NaCl solution was investigated. It demonstrates that the HEA FeCoCrNiMn coating has excellent inherent corrosion resistance. During tribocorrosion tests, frictional frequency plays a significant role in affecting the wear behavior. Although fatigue wear was the dominant wear mechanism at all frequencies varying from 0.5 to 2 Hz, abrasion wear became apparent at high frequencies, especially, at 2 Hz. Quantitative analysis of the corrosion–wear synergy showed that the corrosion augmentation factor increased by 5 times when the tribocorrosion frequency increased from 0.5 to 2 Hz.

Acknowledgments

This work was supported by the State Key Laboratory of Refractories and Metallurgy (Wuhan University of Science and Technology) Open Funding Project (Grant No.G202402), the Open Project Funding of State Key Laboratory for High-Performance Tools (GXNGJSKL-2024-12), the Open Fund of Jiangsu Key Laboratory for Advanced Structural Materials and Application Technology (ASMA202203) and the National Science Foundation of China (Class C) (52503409).

Author Contributions

Fuyang Cao helped in conceptualization, funding acquisition, supervision, writing—review and editing. Mingming Zhang contributed to investigation, data curation, formal analysis, writing—original draft. Hang Wang, Weixuan Sun, Yingqi Sun and Haoquan Wang investigated the study. Hengnan Ding was involved in resources and validation. Fei Wang helped in funding acquisition and writing—review and editing. Rui Luo validated the study. Yu Liu helped in writing—review and editing, funding acquisition.

References

1. J.-W. Yeh, Recent Progress in High-Entropy Alloys, *Ann. Chim. Sci. Mater.*, 2006, **31**, p 633–648.
2. Y. Yu, N.N. Xu, S.Y. Zhu, Z.H. Qiao, J.B. Zhang, J. Yang and W.M. Liu, A Novel Cu-Doped High Entropy Alloy with Excellent Comprehensive Performances for Marine Application, *J. Mater. Sci. Technol.*, 2021, **69**, p 48–59.
3. S.W. Zhan, J.H. Tang, F.T. Wang and X.L. Ji, Tribological Behavior of Laser Clad TiZrHfCrMoW High-Entropy Alloy coating in air and in Simulated Body Solution, *Surf. Technol.*, 2023, **52**, p 29–37.
4. C.J. Cao, Y.F. Wang, C.X. Zhang, D.W. Niu, Y.D. Si, J.J. Si, Z.Q. Shi and Y.L. He, Tribocorrosion Behaviors of Laser Cladding FeCrNiCoMoCuBSi High Entropy Alloy Coating, *Rare Met. Mater. Eng.*, 2023, **52**, p 1439–1446.
5. F.Y. Cao, J.Y. Xie, M.M. Zhang, R. Luo, Q.F. Guan, J.T. Guan, S.Y. Zhou and X.M. Chen, Influence of High Current Pulsed Electron Beam Irradiation on the Microstructure and Mechanical Properties of Nanolayered-TiN/ AlSiN Coatings, *Surf. Coat. Technol.*, 2025 https://doi.org/10.1016/j.surfcoat.2024.131695
6. F.Y. Cao, H.Q. Wang, J.Y. Xie, Z.L. Hao, R. Luo, Z.Z. Yuan, Z.F. Zhou, Z.H. Xie and P. Munroe, Influence of Thickness and Ti Interlayer on Scratch and Wear Resistance of CoCrNi Medium Entropy Alloy Coatings, *J. Mater. Eng. Perform.*, 2025, **34**, p 7386–7395.
7. P.P. Yue, M. Zhang, T. Zhao, P. Liu, F. Peng and L.Q. Yang, Eco-friendly Epoxidized *Eucommia ulmoides* Gum Based Composite Coating with Enhanced Super-Hydrophobicity and Corrosion Resistance Properties, *Ind. Crops Prod.*, 2024 https://doi.org/10.1016/j.indcrop.2024.118523
8. H. Miao, C.H. Yin, H.L. Wang, Y.H. Gao, J.H. Chen, H. Zhang, B. Li, J.S. Wu and K. Xiao, Correlation of Laboratory Simulation Test and Field Exposuretest for Three Stainless Steels in Polluted Marine Atmosphere of Qingdao Coastal Area, *J. Chin. Soc. Corros. Prot.*, 2025, **45**, p 449–459.
9. Y.H. Su, Y. Deng, L.J. Dou and X.W. Liang, Effect of Mo Content on Microstructure and Properties of FeAlCuCrNiMox Alloy, *Transact China Weld Inst*, 2019, **40**, p 111–115+160+166.
10. H. Wu, S.R. Huang, C.Y. Zhu, H.G. Zhu and Z.H. Xie, Influence of Cr Content on the Microstructure and Mechanical Properties of CrxFeNiCu High Entropy Alloys, *Prog. Nat. Sci. Mater. Int.*, 2020 https://doi.org/10.1016/j.pnsc.2020.01.012
11. Z.X. Wang, C. Dong, M.X. Ma, S.Z. Li, L. Zhao and R.S. Hou, Research on Microstructure and Wear Resistance of AlCoCrFeMnTi High Entropy Alloy, *Hot Work. Technol.*, 2023, **52**, p 25–29.
12. P.Y. Shi, Y. Yu, N.N. Xiong, M.Z. Liu and Q.H. Wang, Microstructure and Tribological Behavior of a Novel Atmospheric Plasma Sprayed AlCoCrFeNi High Entropy Alloy Matrix Self-Lubricating Composite Coatings, *Tribol. Int.*, 2020, **151**, p 106470.
13. H.J. Li, W. Zhao, L. Wang, H. Zhang, Y.X. Lv, Z. Wang and W.F. Rao, Effect of Mo-V Co-Addition on the Elastic Properties and Wear Resistance of AlCoCrFeNi High-Entropy Alloy Laser Cladding Coatings, *Intermetallics*, 2025, **187**, p 109016.
14. C.S. Guan, J.J. Fu, Z.C. Cui, S.L. Wang, Q.S. Gao and Y.T. Yang, Evaluation of the Tribological and Anti-Adhesive Properties of Different Materials Coated Rotary Tillage Blades, *Soil Tillage Res*, 2021, **209**, p 104933.
15. X.L. Yu, Q.J. Chen, X. Cui and D.L. Ouyang, Nb-Induced Lattice Changes to Enhance Corrosion Resistance of Al0.5Ti3Zr0.5NbxMo0.2 High-Entropy Alloys, *Nat. Commun.*, 2025, **16**, p 2828.
16. Y.F. Li, A.N. Zou, J. Hu, C.X. Liu, S.X. Zhao, Q.D. Li, W. Zhang and Y.F. Wang, Agricultural Electrostatic Spraying Electrode Corrosion Degradation Mechanisms: A Multi-Parameter Coupling Model, *Agriculture*, 2025 https://doi.org/10.3390/agriculture15131348
17. S.F. Huang, X.L. Zeng, Z. Peng, J. Liu, Z.H. Cai, J. Li, X. Du and J. Liu, Research Progress in High Entropy Alloy Coatings, *Spec. Cast. Nonferrous Alloys*, 2023, **43**, p 876–883.
18. E.Z. Zhou, Y. Yang, J.L. Li, G.Y. Ren, L.K. Li, Z. Li, Y.P. Lu, T.Y. Gu, F.H. Wang and D.K. Xu, A Novel Cu and Ag Bearing High-Entropy Alloy with Remarkable Antibacterial, Antiviral and Anti-Microbial Corrosion Performances, *Adv. Funct. Mater.*, 2025, **35**, p 2419467.
19. G.R. Argade, S.S. Joshi, A.V. Ayyagari, S. Mukherjee, R.S. Mishra and N.B. Dahotre, Tribocorrosion Performance of Laser Additively Processed High-Entropy Alloy Coatings on Aluminum, *Appl. Phys. A*, 2019, **125**, p 272.
20. G.W. Huang, L.X. Li, J. Cheng, W.Y. Chen, J.J. Chen, S.Y. Zhu and J. Yang, Tribological Behavior of Detonation Sprayed CrFeNiAl_(0.3)-Ti_(0.3) High Entropy Alloy Coatings in Seawater Environment, *Tribol. Int.*, 2024, **194**, p 109480.
21. F.Y. Luo, S.S. Wang, W.Q. Shi, Z.Y. Xiong and J. Huang, Analysis of the Wear Behavior and Corrosion Resistance of CoCrFeNiMn-2% CNTs Laser Cladding Composite Coating, *J. Mater. Res. Technol.*, 2024, **30**, p 6910–6923.
22. L. Lu, J.W. Wang, Q.S. Du, W. Diao, W.H. Wen, B. Cheng, L.Y. Dai and L.J. Yang, Corrosion and Wear Behaviors of High Entropy alloyAlCoCrFeNi Coating Prepared by HVOF, *Chin. J. Nonferrous Met.*, 2025, **35**, p 1402–1415.
23. F. Cao, H. Wang, Q. Ji, H.N. Ding, Z.Z. Yuan and R. Luo, Tribo-Corrosion Performance of Atmospheric Plasma Sprayed FeCoCrNiMn High Entropy Alloy Coatings, *J. Chin. Soc. Corros. Prot.*, 2024, **44**, p 1529–1537.
24. C. Cao, K.T. Li, J.Z. Ye, F.S. Guo, Q.P. Yu, Effect of Addition of Mo and Nb2O5 on Microstructure and Mechanical Properties of Plasma Sprayed Chromium Oxide-based Coating, Surf. Technol., 2025, pp.1–14
25. B.N.J. Persson, *Sliding Friction: Physical Principles and Applications*, Second Edition. Springer, Berlin, 2000
26. S.J. Zheng, Z.B. Cai, J.B. Pu, C. Zeng and L.P. Wang, Passivation Behavior of VAlTiCrSi Amorphous High-Entropy Alloy Film with a High Corrosion-Resistance in Artificial Sea Water, *Appl. Surf. Sci.*, 2021, **542**, p 148520.
27. Y.C. Wu, Z.W. Wang, J.L. Chen, Y.L. Ma, Y. Yan and L.J. Qiao, Effect of Frictional Frequency on the Subsurface Evolution of 316L Stainless

Steel in Tribocorrosion and its Influence on the Synergistic Effect Between Corrosion and Wear, *Tribol. Int.*, 2023, **178**, p 108026.
28. Q. Feng, P.W. Ren, H. Liu, Y.H. Shi and J.Z. Wang, Frequency-Dependent Fretting Tribocorrosion Mechanisms of Ti6Al4V Alloy in Seawater, *Surf. Coat. Technol.*, 2025, **517**, p 132798.
29. B.S. Lou, I. Rahmadtulloh, C.J. Wang, W.H. Wang and J.W. Lee, Tribocorrosion Behaviors of VNbMoTaWCr High Entropy Alloy Coatings, *Surf. Coat. Technol.*, 2024, **476**, p 130250.
30. Y. Ge, J. Cheng, L. Xue, B. Zhang, S. Hong, X. Liang, S. Wang and X. Zhang, Pore Defect and Corrosion Behavior of HVAF-Sprayed Co21Fe14Ni8Cr16Mo16C15B10 High Entropy Metallic Glass Coatings, *Corros. Sci.*, 2025, **242**, p 112564.
31. J. Chen, Q. Zhang, Q.-A. Li, S.-L. Fu and J.-Z. Wang, Corrosion and Tribocorrosion Behaviors of AISI 316 Stainless Steel and Ti6Al4V Alloys in Artificial Seawater, *Trans. Nonferrous Met. Soc. China*, 2014, **24**, p 1022–1031.
32. Y.Z. Zhao, X.C. Li, L. Gao, L. Jiang and Z.Q. Cao, Effects of Sintering Temperature on Microstructure and Properties of (AlCoCrFeNi2.1)p/Cu Composites, *Spec. Cast. Nonferrous Alloys*, 2022, **42**, p 1511–1517.
33. L.T. Wang, D. Mercier, S. Zanna, A. Seyeux, M. Laurent-Brocq, L. Perrière, I. Guillot and P. Marcus, Study of the Surface Oxides and Corrosion Behaviour of an Equiatomic CoCrFeMnNi High Entropy Alloy by XPS and ToF-SIMS, *Corros. Sci.*, 2020, **167**, p 108507.